Desalination and Water Treatment
www.deswater.com
doi: 10.5004/dwt.2023.30095

315 (2023) 49–61
December

Adsorptive methylene blue removal using modified agricultural wastes

Yasemin İşlek Coşkun

Department of Chemistry, Faculty of Science, Ege University, Bornova, Izmir, Turkey, Tel.: +90(232)3112389; Fax: +90(232)3888294; email: yasemin.islek@ege.edu.tr (ORCID ID: 0000-0003-3207-4381)

Received 8 February 2023; Accepted 23 October 2023

ABSTRACT

A magnetic nano biocomposite was developed by coating the surface of pressed *Nigella sativa* press cakes agricultural waste with Fe_3O_4 nanoparticles. The uptake of methylene blue from an aqueous solution was evaluated. pH, adsorbent dosage, interaction time, and other parameters were investigated. Equilibrium, kinetic, and thermodynamic models were analyzed. Desorption studies were performed using various solvents. The uptake efficiency of methylene blue reached 93.22% at pH 11. The adsorbent dosage was determined as 0.6 g/L. The uptake efficiency reached 99.40% at 24 h. Adsorption mechanism is found to be both endothermic and spontaneous. The rate-determining step of adsorption is chemical sorption. The adsorption capacity was 454.55 mg/g. Desorption was performed by ethanol and reached 49.21%. The adsorption performances of the adsorbent were also evaluated by real water samples. Toxic and hazardous reagents were not handled in the preparation of the adsorbent. An environmentally friendly, easily prepared, cheap adsorbent has been developed.

Keywords: Methylene blue; Dyes; Adsorption; Nanostructures; *Nigella sativa*; UV/Vis spectroscopy

1. Introduction

Humans have used dyes for many purposes since ancient times. Nowadays, they are used in textiles, dyes, paper, pulp, tanning, and the dye industry. The discharge effluent of these industries contains significant amounts of dye compounds considering that they are poisonous, the removal of dyes before discharge is important [1,2]. Dyes cause various health problems including tachycardia, nausea, dizziness, jaundice, tissue death, and allergies [2].

Synthetic dyes, especially cationic dyes (basic dyes), are stable, non-biodegradable, aromatic compounds. Methylene blue dye is a basic (cationic) dye [1]. A variety of techniques have been used to eliminate dyes from aqueous media. Filtration, chemical treatment, oxidation, electrochemical techniques, sophisticated oxidation systems, biological processes, and adsorption are among the most important [1–4]. Alumina, silica gel, zeolites, active carbon, natural materials, industrial, agricultural and domestic wastes, composites, and nanomaterials are used to remove dyes [3,5,6].

Cost is an important factor in adsorbent comparison. Natural adsorbents are abundant and can be used as adsorbents after some physical or chemical pretreatment. Furthermore, these materials possess cellulose surfaces containing substantial functional groups that attract metal ions, resulting in composite formation [7]. *Citrus limetta* peel and *Zea mays* cob were used to eliminate malachite green, methylene blue, and Congo red dyes. The materials were handled with distilled water to remove contaminants. Then, they were dried under-the sun for between 5 and 7 d. The adsorption capacity was 8.77 and 16.7 mg/g for *Citrus limetta* peel and *Zea mays* cob, respectively [8]. The drawback of natural materials is that it is difficult to separate the adsorbent from the solution medium. This problem can be overcome by modifying the surface of the natural material with magnetic components. Thus, the adsorbent can be

* Corresponding author.

separated from the medium by applying a magnetic field [9]. Magnetic nanomaterials offer exceptional magnetic characteristics, increased surface area, affordability, the potential for reuse, and effortless separation. In the synthesis of magnetic adsorbents, magnetite nanoparticles are commonly utilized as magnetic agents for the separation of metal ions and organic pollutants. [10,11]. Manganese ferrite composite biomaterial was synthesized on *Nigella sativa* seeds, and the prepared magnetic adsorbent was used for methylene blue dye adsorption. The reported adsorption capacity was 74.63 mg/g [7]. Magnetite was synthesized on vine shoots derived activated carbon for the removal of Cr(VI) and admirable adsorption capacity was reported as 305 mg/g. [11].

Black cumin is cultivated within Turkish regions like Mersin, Gaziantep, and Isparta. In Türkiye, pressed black cumin (*Nigella sativa*) cake represents an agricultural solid waste material, obtained after mechanically cold pressing black cumin seeds. This press cake is both economical and readily available. However, improper disposal of the press cake leads to significant waste-related issues [12]. According to the literature, black cumin seed (*Nigella sativa* L.) has been applied to remove both organic contaminants and metals from aqueous solutions. *Nigella sativa* seeds have been used for methylene blue (MB) removal after being physically modified (heated at different temperatures) [13] and acid washed [14]. Various nano biocomposites based on *Nigella sativa* have also been developed and utilized for MB removal, heavy metal removal, and antibacterial activity [15–19]. Nonetheless, to the best of our knowledge, our previous study is the first study on pressed black cumin press cakes for adsorption/removal of Cu(II) from an aqueous solution [20]. According to our investigation, there is no study which the surface of the black cumin pressed cake was modified by Fe_3O_4 particles for MB adsorption. By this modification it is aimed that both the difficulties encountered in the separation of natural materials from the solution medium will be eliminated and the superior properties of the magnetic particles are utilized. *Nigella sativa* seeds could have released the extract containing phytochemicals, which might have also functioned as stabilizing and capping agents, thereby yielding nanosized particles [9]. The biomass performs as a dispersing or capping agent, preventing magnetite nanoparticles from agglomerating and thereby reducing surface reactivity [21,22]. The newly prepared adsorbent was superior to the above-mentioned *Nigella sativa*-based composites. This may be due to increased pore numbers after mechanical pressure. The efficiency of the adsorbent was evaluated by investigating pH, adsorbent dose, contact time, and kinetic, thermodynamic, and equilibrium studies.

2. Experimental set-up

The chemicals used were all analytical grade. Ultrapure water was utilized throughout the study. Methylene blue, HCl (hydrochloric acid), NaOH (sodium hydroxide), $FeCl_3{\cdot}6H_2O$ (iron(III) chloride hexahydrate), $(NH_4)_2Fe(SO_4)_2$ (ammonium iron(II) sulfate), acetone, ethanol, and methanol were supplied by Merck (Germany).

Stock methylene blue solution (1,000 mg/L) was prepared by dissolving aliquot amounts of methylene blue in ultra-pure water. Model solutions were prepared daily after diluting stock methylene blue solution.

All glassware and polypropylene materials were soaked in 10% nitric acid (HNO_3) solution for a night and washed in distilled water before use.

Black cumin seeds were mechanically pressed and yielded the black cumin pressed cake, and it was purchased from a supplier in Dikili-Izmir.

2.1. Apparatus

A pH meter was used for adjusting the pH of the solutions (Mettler Toledo FiveGo FG-2, Germany). The adsorption studies were executed by using a vibration water bath (Nuve ST-402, Turkey) and an orbital shaker at 350 rpm (Biosan OS-10, Latvia). The absorption measurements of methylene blue were carried out using a PG Instruments TG 80+ model UV-Vis spectrophotometer (UK) (double beam) at 663 nm. Fourier-transform infrared spectroscopy (FTIR) examinations of the magnetite-nano biocomposite were performed between 4,000 and 400 cm^{-1} (PerkinElmer 100, USA). The scanning electron microscopy (SEM) analysis for surface morphology and energy-dispersive X-ray spectroscopy (EDX) was carried out by Thermo Fisher Scientific Apreo S LoVac (USA). Rigaku SmartLab X-ray Diffractometer with Cu-Kα radiation (λ = 1.54 Å, 40 kV, 40 mA) (Japan) was used to determine the crystal structure. Determination of surface area and pore structure were carried out by QuantaChrome Autosorb iQ2 (USA). Zeta potential measurement was executed by Malvern Panalytical Zetasizer ZS XPLORER, UK.

2.2. Preparation of the magnetic nano biocomposite

Pressed *Nigella sativa* seed cakes were obtained after the cold press of *Nigella sativa* seeds. The press cake was ground in a mortar. The ground press cake was then washed with boiling distilled water till supernatant becomes clear. It was dried overnight at 80°C and sieved at 350–500 μm.

To obtain magnetite coating, 2 g of press cake was taken and added to $FeCl_3$ and $(NH_4)_2Fe(SO_4)_2$ (mole ratio 2:1). 100 mL of distilled water was added. Nitrogen gas was passed through the solution for 30 min. Next, the temperature of the solution was set to 80°C and 2 mol/L 40 mL of NaOH solution was added drop by drop [23]. The solution turned black. N_2 gas was passed through the solution for another 30 min. Subsequently, the adsorbent was treated several times with distilled water until the pH became neutral and ethanol. Finally, the adsorbent was dried in an oven at 60°C for 24 h. The prepared adsorbent was placed in a polypropylene container. The prepared material was named MNYBC (magnetite modified black cumin composite).

2.3. Batch uptake studies

The uptake studies were realized with the batch method. The parameters were investigated using 25 mL of dye solution. The initial dye concentration and contact time were 20 mg/L and 24 h. The amount of MNYBC was 10 mg in the pH study. After the optimization study, the adsorbent dosage was determined to be 0.6 g/L. In the optimization studies, pH, MNYBC dosage, contact time, and the impacts

of temperature were examined. The isotherm study was performed in the range of 0.1–5,000 mg/L of concentration. The kinetic models were studied for between one and 1,440 min. The magnetic adsorbent was separated from the model solution by an external magnetic field. Unadsorbed dye concentrations were measured by UV-Vis spectrophotometer at 663 nm. The experiments were performed in triplicate. The uptake efficiencies (R, %) and capacities (q, mg/g) were computed using the Eqs. (1) and (2), respectively:

$$R(\%) = \frac{(C_i - C_e)}{C_i} \times 100 \quad (1)$$

$$q\left(\text{mg g}^{-1}\right) = \frac{(C_i - C_e)}{w} \times V \quad (2)$$

where C_i and C_e indicate initial and equilibrium MB concentration (mg/L), w is MNYBC amount (g), V is the volume of the solution (L).

3. Results and discussion

3.1. Characterization studies

FTIR measurements were performed to detect possible functional groups taking part in the adsorption processes. The FTIR spectra that were obtained pre and post uptake are seen in Fig. 1. Before adsorption, the band at about 3,400 cm^{-1} could belong to O–H stretching vibrations [24,25]. The change observed could indicate hydrogen bonding between the adsorbent and dye molecules. The peaks at 2,924.52 and 2,924.70 cm^{-1} could refer to C–H stretching vibrations belong to $–CH_2$ and $–CH_3$ groups [24–26]. The peaks between 1,670 and 1,640 cm^{-1} might belong to C=O stretching vibrations of carboxyl, ketone, and aldehyde groups [24,26,27]. The shifting from 1,633.82 to 1,604.02 cm^{-1} after adsorption could mean that the carbonyl groups take part in the adsorption. The bands at 1,416.89 and 1,389.15 cm^{-1} may imply the stretching vibrations of C=C [26]. The peaks at 1,088 and 1,057.22 cm^{-1} could indicate C–O–C and C–O stretching vibrations [28]. Fe–O vibrations were presented by the vibrations at 584.81 and 582–631.60 cm^{-1} before and after adsorption, respectively [29,30]. The presence of that peak is also an evidence of magnetite bonding on the surface of MNYBC. The intensities of Fe–O vibration bands were observed to increase following adsorption, suggesting the involvement of associated groups in the adsorption process [31]. Also, the presence of a divided Fe–O band in MB-loaded MNYBC indicated a partial distribution in the arrangement of vacancies [32]. The changes observed in the FTIR bands attributed to adsorbent after MB adsorption indicate an interaction between the adsorbent surface and MB, likely mediated by electrostatic and/or H-bonding [7,22,33]. The results are found to be consistent with the literature [7,9,31,34].

The SEM and EDX data of the MNYBC were collected before and after MB dye adsorption. The related images are expressed in Fig. 2. In the figure it is clearly seen that the synthesized magnetite settled on these honeycomb-like structures as small ball-like structures. It was observed that some parts of this structure were covered by a smoother surface after MB adsorption. The chemical characterization of the surface was determined by EDX to be 20.21% C, 33.8% O, 43.34% Fe, and 2.65% N before adsorption, and 43.65% C, 16.92% O, 19.66% Fe, 7.07% N, and 12.7% S by weight after adsorption. Sulfur occurring on the surface and nitrogen, which was observed to increase on the surface after adsorption, may be caused by the adsorption of the MB. Decrease in the iron amount could also be the result of adsorption of MB. Since MB covered the surface of the adsorbent, iron might not be detected by the EDX detector.

The method used to state the point of zero charge was that of Fiol and Villaescusa [35]. It is thought that when the pH value was below the pzc value, the adsorbent surface had a positive charge thus the adsorbent surface impelled away the positive charged methylene blue dye molecules.

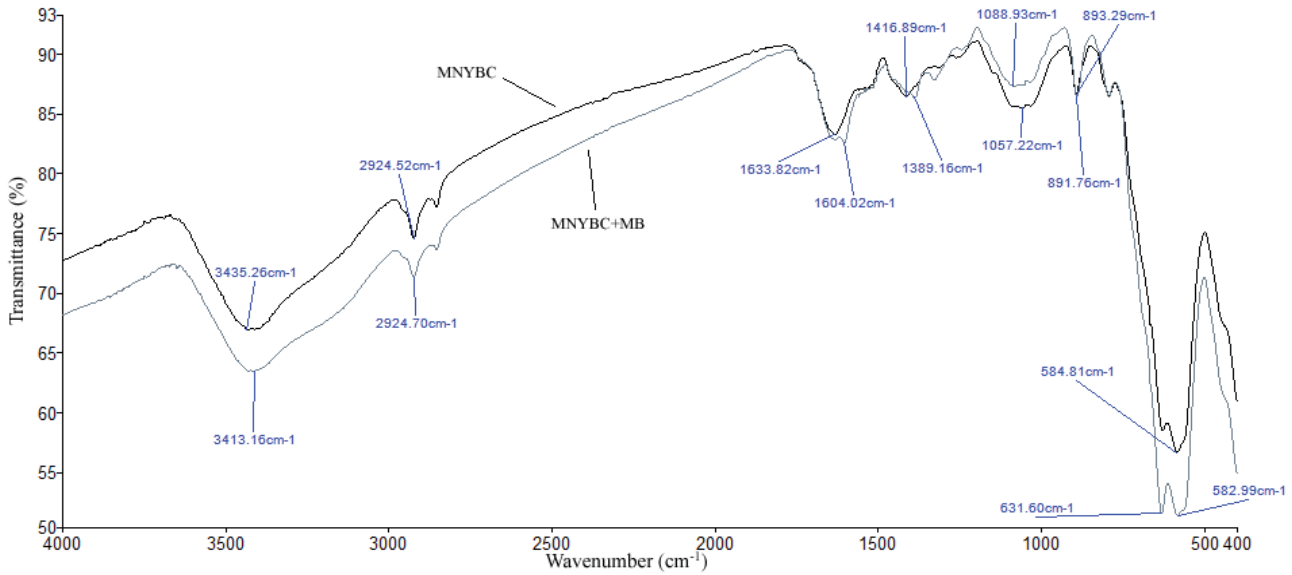

Fig. 1. Fourier-transform infrared spectra of MNYBC before and after methylene blue uptake.

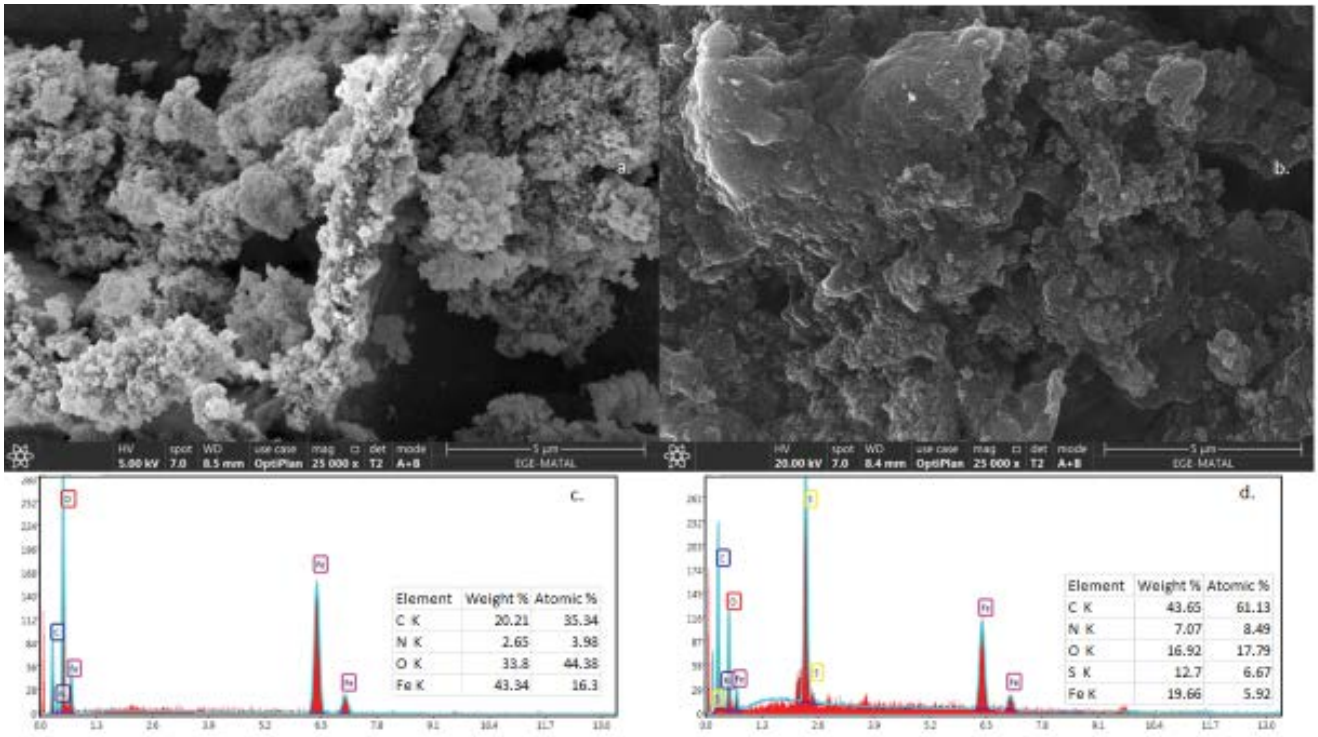

Fig. 2. Scanning electron microscopy and energy-dispersive X-ray spectroscopy images of the MNYBC before (a,c) and after methylene blue uptake (b,d).

Finally, the uptake efficiency decreases. Above the pzc value, the surface of the adsorbent is negative charged, and attracts the positive charged dye molecules. The point of zero charge (pzc) of modified adsorbent and bare adsorbent were found to be 6.20 and 5.31, respectively. The pzc value of MNYBC was supported by the value reported by Petrova et al. [36], which falls between 6 and 6.8. The change in pzc value after coating the bare *Nigella sativa* press cake with magnetite is due to the presence of iron oxides, which have a pH range of approximately 8–9. As a result, in Fig. 3 pH values above six, the uptake efficiencies increased. The adsorption of the MB dye could be based on electrostatic attractions [7]. Similar attractions were taken place was reported [7,31]. Besides, zeta potential of the magnetic adsorbent was determined as –22.59 mV. This value is consistent with the literature [37].

The X-ray diffraction patterns of both virgin black cumin press cake and MNYBC displayed characteristic peaks within the 10°–80° (2θ) range. These patterns are illustrated in Fig. 3. In Fig. 3a the X-ray diffraction pattern of black cumin press cake exhibited a broad peak between 20°–24° (2θ) associated with the (002) plane. This peak arises from the amorphous region of cellulose within the black cumin press cake, as reported in the literature. [7,15,38]. The disappearance of this peak indicates the formation of magnetite on the press cake's surface [15,38]. Additionally, peaks observed at 30.18°, 35.587°, 43.34°, 53.57°, 57.22°, and 62.84° correspond to the (220), (311), (400), (422), (511), and (440) planes of the Fe_3O_4 crystal structure, respectively. The presence of the peak at 35.587° further confirms the Fe_3O_4 phase (2θ = 35.423) (JCPDS file no. 19-629) [22,38]. Similar patterns

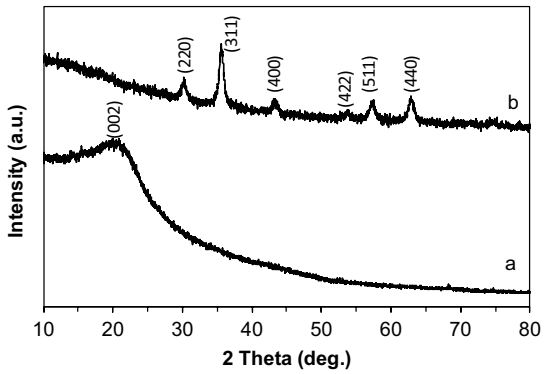

Fig. 3. X-ray diffraction spectra of bare black cumin pressed cake (a) and MNYBC (b).

were reported by other researchers [22,34,38]. Utilizing the Debye–Scherrer equation [Eq. (S9)], the average size of the MNYBC composite nanoparticles was calculated to be 10.30 nm. The BET results revealed that the surface area of the adsorbent was 60.64 m^2/g, the total pore volume 4.56×10^{-1} cm^3/g, and the average pore radius 1.51×10^2 Å.

3.2. Impact of pH on the uptake efficiency

pH is a critical factor that affects the uptake process. The impact of pH on the methylene blue solution was examined in the range of 3–11. The initial concentration was set to 20 mg/L. 10 mg was weighed and put into falcon tubes. Then, 25 mL of MB solutions were added. The MNYBC and

model solutions were shaken for 24 h in an orbital shaker (320 rpm). A magnet was used to separate the MNYBC from the model dye solution. After separation, the model MB solutions were acidified and then, unadsorbed dye concentrations were determined. The results are depicted in Fig. 4a. The highest uptake efficiency was obtained at pH 11 with 93.22% ± 0.67%. The highest uptake efficiencies at basic pH were also reported for MB removal [7,34]. An increase in adsorption capacity was observed to correspond with an increase in pH. Similar results were obtained in other studies [34]. At pH 11, adsorption capacity reached 48.03 mg/g.

3.3. Impact of the MNYBC dosage on uptake efficiency

The impact of the MNYBC dosage on methylene blue removal by magnetite coated nano biocomposite was investigated. The studied adsorbent dosages were 0.2, 0.4, 0.6, 0.8, 1.6, and 2.0 g/L. 25 mL of 20 mg/L MB solution at pH 11 was added to the adsorbents and shaken for 24 h. The results are shown in Fig. 4b. The optimum adsorbent dosage was found to be 0.6 g/L. Jiang et al. [39] synthesized magnetic sugarcane-bagasse activated carbon for MB removal and reported that the optimum adsorbent dose was 5 g/L. It has been also reported that MB removal was carried out by 0.02 g of manganese ferrite/graphene oxide nanocomposites [40].

According to Fig. 4b, the MB uptake efficiencies were not significantly affected by the MNYBC dosage. The uptake efficiency for 0.2 g/L was 92.84% ± 0.19%. With 0.4 and 0.6 g/L adsorbent dosages, this increased to 98.10% ± 0.30% and 99.20% ± 0.19%, respectively. The uptake efficiencies increased with increasing numbers of active sites in the magnetite coated nano biocomposite, and reached a constant value [34]. This could be the result of increased numbers of pores in the structure of the natural material caused by mechanical pressure. In addition, as the adsorbent dosage increases, a decrease in adsorption capacity is observed. This is due to the increase in the vacant sites as the adsorption amount rises, while the existing MB quantity cannot fill these sites [11]. Similar tendency was reported in the literature [11,21,34]. Because of this, the capacity was decreased from 92.89 to 8.25 mg/g. Furthermore, the effect of adsorbent dosage on pH variation was explored within the range of 0.2–2.4 g/L, revealing no discernible correlation between the two factors. The related figure can be seen in Fig. S1.

3.4. Impact of contact time on the uptake efficiency and kinetic models

The impact of contact time on the uptake efficiency of methylene blue was studied for 1, 5, 10, 20, 40, 60, 120, 180, 300, and 1,440 min. 25 mL of 20 mg/L MB model solution at pH 11 was added to 0.6 g/L of magnetite nano biocomposite and shaken for the stated time intervals. Unadsorbed MB concentrations were measured. The impact of contact time on the uptake efficiency is depicted in Fig. 5a. The uptake ratio was relatively high. In addition, 83.15% ± 3.14% of MB dye was adsorbed within the first 20 min. This phenomenon was related to the higher number of active sites of the adsorbent at the beginning of the adsorption process.

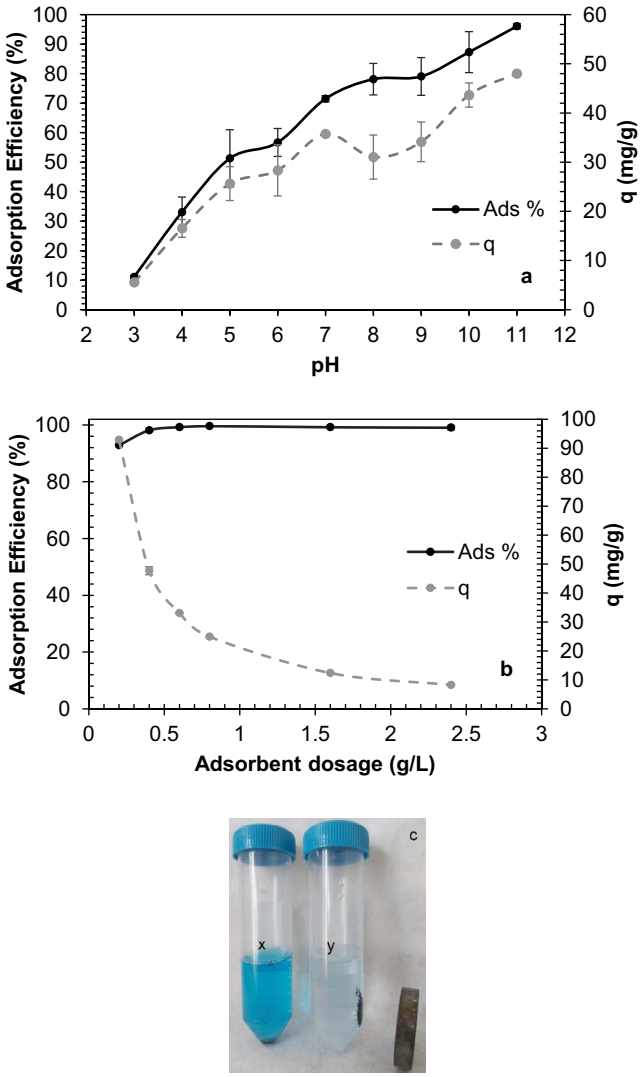

Fig. 4. Impact of pH (a) and adsorbent dosage (b) on the methylene blue uptake and image of magnetic separation of MNYBC (c).

The adsorption rate will decrease as these active sites are occupied by MB dye molecules [34]. The highest uptake efficiency was reached at 1,440 min with 99.40% ± 0.05%. Furthermore, a similar pattern to the uptake efficiency graph was obtained for the uptake capacity, where it initially increases rapidly with time and then then reached a constant value. The maximum uptake capacity was 16.56 mg/g.

Three kinetic models were used to study the mechanism of adsorption: Lagergren pseudo-first-order, Lagergren pseudo-second-order, and the intraparticle diffusion model [41,42]. These models depict external film diffusion, adsorption, and the adsorption's intraparticle diffusion ratio. Fig. 5 illustrates the pseudo-first-order, pseudo-second-order, and intraparticle diffusion graphs (b–d). The related equations and the computed constants are tabulated in Table 1.

Table 1 depicts that the highest coefficient of determination (R^2) was acquired for the pseudo-second-order model. Furthermore, the predicted and experimental adsorption

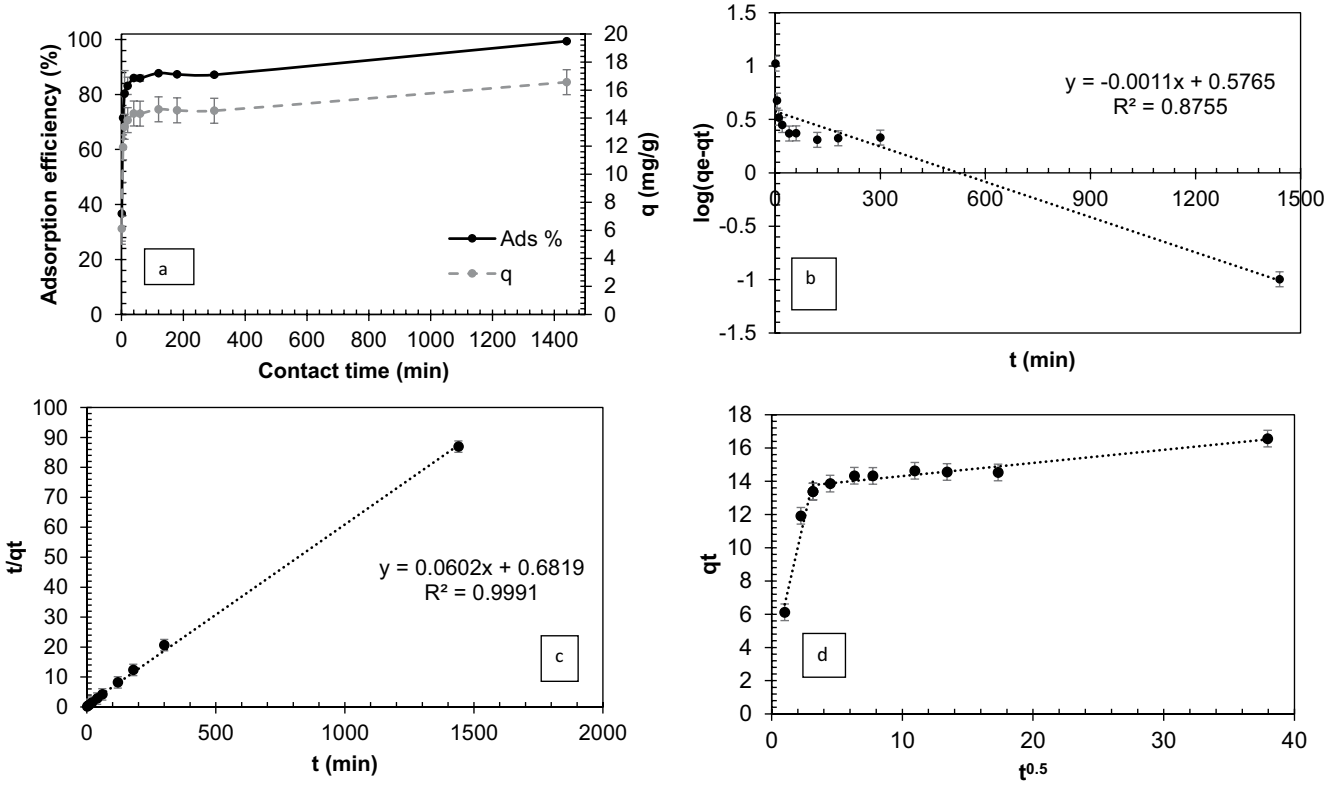

Fig. 5. Impact of contact time on the methylene blue uptake (a), pseudo-first-order (b), pseudo-second-order (c), and the intraparticle diffusion (d) (initial concentration of methylene blue model solution 20 mg/L, volume 25 mL, adsorbent dosage 0.6 g/L, contact time range 1–1,440 min, pH 11, $n = 3$).

Table 1
Constants of pseudo-first-order, pseudo-second-order, and the intraparticle diffusion for methylene blue adsorption on MNYBC

Kinetic models	Equation	Constants	
Pseudo-first-order	$\log\left(q_e - q_t\right) = \log q_e - \frac{k_1 t}{2.303}$	$q_{e,\exp}$ (mg/g)	16.67
		$q_{e,\text{cal}}$ (mg/g)	3.77
		k_1 (1/min)	0.00253
		R^2	0.8755
Pseudo-second-order	$\frac{t}{q_t} = \frac{1}{k_2 q_e^2} + \frac{t}{q_e}$	$q_{e,\text{cal}}$ (mg/g)	16.61
		k_2 (g/mg·min)	0.00531
		R^2	0.9991
Intraparticle diffusion	$q_t = k_{\text{int}} t^{0.5} + I$	Stair 1	
		I_1 (mg/g)1	3.1531
		k_{id1} (mg/g·min$^{0.5}$)	3.4319
		R^2	0.9388
		Stair 2	
		I_2 (mg/g)	13.521
		k_{id2} (mg/g·min)	0.079
		R^2	0.9205

Adsorption capacities at equilibrium and at time t are denoted by q_e and q_t (mg/g). Pseudo-first-order, pseudo-second-order and intraparticle diffusion rate constants k_1 (1/min), k_2 (g/mg·min) and k_{id} (mg/g·min$^{0.5}$). I (mg/g) is the intraparticle diffusion constant.

capacities were incredibly similar. These results imply that the adsorption kinetic complied with the pseudo-second-order. The rate-determining stage was chemical sorption controlled [43]. Based on the intraparticle diffusion model (Fig. 5d and Table 1), high correlation coefficients were also discovered. This highlighted the influence of the

intraparticle diffusion model on the adsorption process. However, in Fig. 5d, the plot not starting from the origin indicated that the rate-limiting mechanism wasn't exclusively determined by intraparticle diffusion. The presence of two lines suggested a two-step adsorption process (film diffusion and intraparticle diffusion). Analyzing lower K_d and higher boundary layer (I) values provided insight into which stair governed the adsorption rate. In Table 1, it is evident that stair 2 had a lower K_d value and a higher I value, indicating the dominance of intraparticle diffusion in the adsorption process. This finding aligns with results in existing literature [7].

In a nutshell, the current process of MB adsorption adheres to pseudo-second-order kinetic model and involves intraparticle diffusion. This implies that the adsorption operates through chemisorption and is constrained by intraparticle diffusion. The results obtained here are consistent with the results obtained from the isotherm studies, where the isotherm results indicate adherence to the Langmuir isotherm, implying chemical sorption. The FTIR spectrum of MB loaded MNYBC (Fig. 1) indicated potential mechanisms, namely electrostatic and non-electrostatic interactions. Similar adsorption mechanisms were reported by other authors [32]. Possible binding mechanism of MB on MNYBC can be seen in Fig. 6.

3.5. Impact of temperature on uptake efficiency and thermodynamic models

The impact of temperature on the uptake efficiency of MB was examined at 20°C, 30°C, 50°C, and 70°C. Thermodynamic studies indicates the impact of temperature on the uptake process. The related equations are given in the Supporting Information. The results are tabulated in Tables 2 and S2 for MNYBC and bare adsorbent, respectively.

The negative $\Delta G°$ values in Table 2 show that the adsorption was spontaneous and favorable. The positive $\Delta S°$ values highlighted randomness increases during the adsorption process. In addition, positive enthalpy changes indicated the adsorption was endothermic. That value was above 60 kJ/mol showing the presence of chemical interplay on the adsorption [44].

It has been reported that the MB adsorption on magnetic sugarcane bagasse-activated carbon and activated carbon

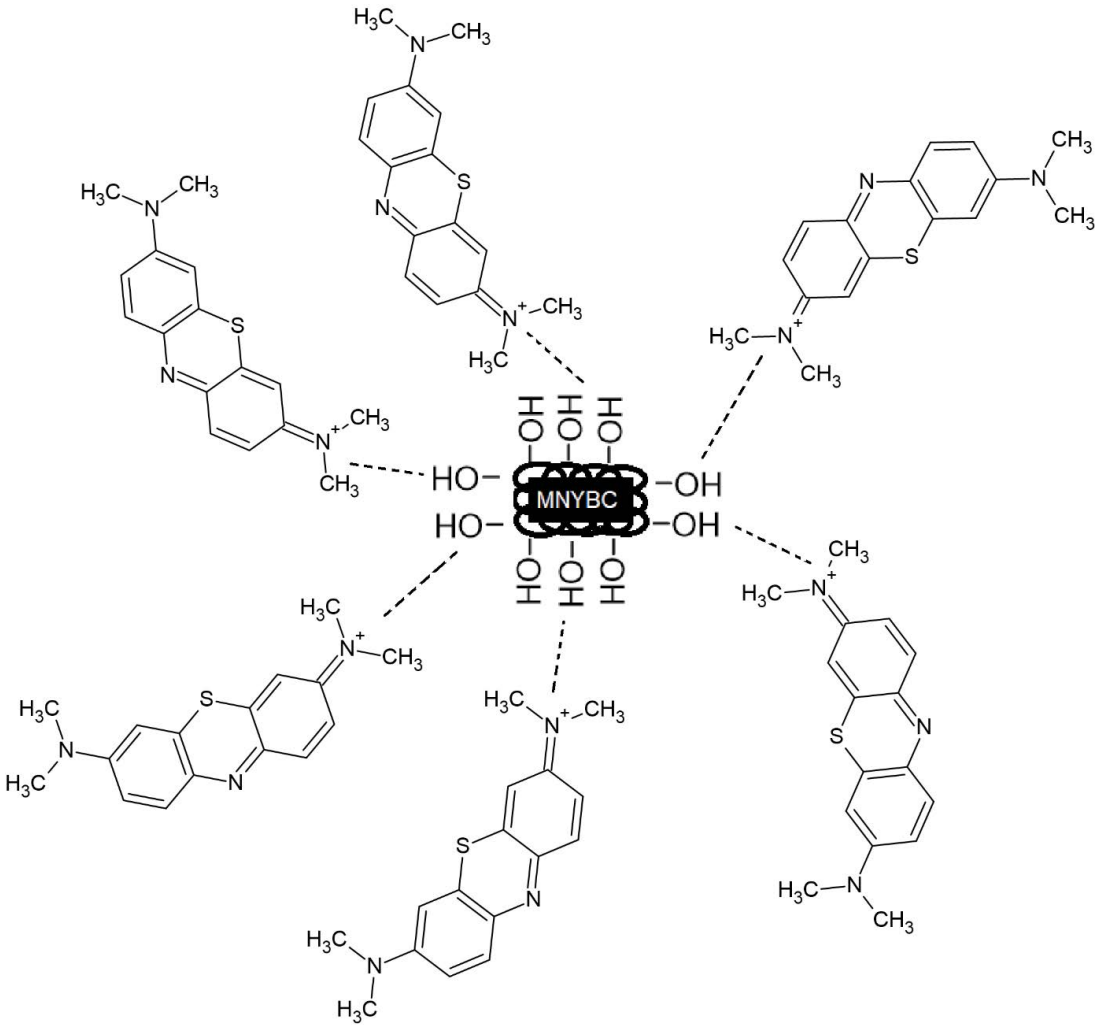

Fig. 6. Predicted binding mechanism of methylene blue on MNYBC.

Table 2
Thermodynamic constants for the adsorption of methylene blue

Temperature (K)	Standard enthalpy changes (kJ/mol)	Standard entropy changes (J/mol·K)	Gibbs free energy changes (kJ/mol)
293	88.53	329.4	–7.980
303			–11.27
323			–17.86
343			–24.45

derived from black cumin was also endothermic and the adsorption process was spontaneous [33,39].

3.6. Impact of initial MB concentrations on uptake efficiency and equilibrium studies

Isotherm studies clarify the interactions between MB dye molecules and the adsorbent as well as the nature of the interactions. The experimental findings were applied into the Langmuir, Freundlich, and Dubinin–Radushkevich isotherm models [45,46]. Detailed information about isotherm models and related equations are given in the Supporting Information. Initial MB dye concentrations between 0.1 and 5,000 mg/L were investigated. Tables 3 and S1 represents the constants for MNYBC and bare adsorbent, respectively.

The coefficient of determination is used to express the isotherm model that best fits the system. The Langmuir isotherm model had the highest coefficient of determination, as seen in Table 3. Uptake on the MNYBC surface is assumed to be monolayer and homogeneous. The highest adsorption capacity was computed as 454.55 mg/g. The result of $1/n$ defines the intensity of the adsorption. As the $1/n$ value improves, then the interactions between the MB and the adsorbent enhance. The separation factor (R_L) indicates that the adsorption is favorable ($0 < R_L < 1$), unfavorable ($R_L > 1$), linear ($R_L = 1$), or irreversible ($R_L = 0$) [10]. The mean free energy of adsorption (E, kJ/mol) describes the mechanism of the uptake process. Values below 8 kJ/mol suggest physical adsorption, while values between 8 and 16 kJ/mol indicate ion exchange, and values above 16 kJ/mol correspond to chemical sorption [10,21]. In this study, the E value was found to be 9.05 kJ/mol, indicating the presence of ion exchange mechanism. The comparison table of maximum monolayer adsorption capacity of MB removal studies found in the literature is tabulated in Table 4. Compared to other adsorbents in the literature, MNYBC stands out with its low adsorbent dosage and high-capacity value, despite its long adsorption time.

Table 3
Parameters determined for the Langmuir, Freundlich, and Dubinin–Radushkevich isotherms

Isotherm models		
Langmuir isotherm	Q_{max} (mg/g)	454.55
	b (L/mg)	0.0037
	R^2	0.9208
	Separation factor (R_L)	0.9996–0.0512
Freundlich isotherm		
	$1/n$	0.6661
	K (mg/g)	4.68
	R^2	0.8445
Dubinin–Radushkevich isotherm	E (kJ/mol)	9.05
	Q_m (mol/g)	0.0040
	K (mol²/kJ)	0.0061
	R^2	0.9452

3.7. Desorption of MB from the adsorbent

MB desorption was examined under the following conditions: 0.6 g/L of adsorbent dosage, 25 mL of volume, 20 mg/L of MB dye concentration, and 1,440 min of contact time. The uptake efficiency was calculated as 99.8% ± 0.9%. Then, the unadsorbed dye molecules were eliminated by washing the adsorbent in distilled water. The solvents used for desorption were ethanol, methanol, and acetone. 10 mL of solvent was added to the loaded adsorbent and agitated for 1,440 min. The desorption efficiencies were calculated as 49.21% ± 0.75%, 37.05% ± 0.87%, and 37.22% ± 1.22% for ethanol, methanol, and acetone, respectively. According to isotherm models and kinetic studies, the adsorption of MB on magnetite nano biocomposite was based on chemisorption. Interactions between dye molecules and the adsorbent are stronger for chemisorption. It is difficult to desorp the dye molecule retained by this bond from the solid surface [1,2]. That phenomenon could be an explanation for low desorption efficiencies.

3.8. Application to real samples

The adsorption performances of the prepared MNYBC were evaluated by applying the adsorbent to real water samples: wastewater which is taken by dye industry (chemical oxygen demand: 5,005 mg/L, total suspended solid: 566 mg/L, pH 11.42), tap water, and distilled water. The all-water samples were spiked with 1, 10, and 100 mg/L of MB solution. The results are tabulated in Table 5. The spiked MB was effectively removed by the adsorbent.

3.9. Comparison study

The performance of the magnetically modified black cumin press cakes is compared to other studies in the literature in Table 4. According to Table 4, the MNYBC was superior to the other adsorbents in having the lowest adsorbent dosage and the highest adsorption capacity. As compared

Table 4 Comparison chart of the carbon-based magnetic adsorbents reported in the literature

Adsorbent	Optimum pH	Optimum dose (g/L)	Contact time (min)	Adsorption capacities (mg/g)	Kinetic models	Isotherm models	References
$MNFe_2O_4$/rGO-BC	8–10	1	120	74.63	PSO	Freundlich	[7]
Acid washed nigella sativa seed powder	7–10	1	30	73.529	PSO	Langmuir and Freundlich	[14]characterization of a green natural product-based adsorbent, acid washed black cumin seeds (AWBC
Nigella sativa based-$MnFe_2O_4$/BC	7–10	3	45	10.07	PSO	Langmuir	[15]
Nigella sativa based-MnO_2/BC	7	1	60	185.185	PSO	Freundlich	[16]
Nigella sativa based-Fe_2O_3-SnO_2/BC	7	2	90	58.82	PSO	Freundlich	[17]
Nigella sativa graphene oxide-based nanocomposite	7	1	150	125	PSO	Freundlich	[18]
Fe_3O_4@date seeds powder	8–10	1	90	76.65	PSO	Freundlich	[34]
Magnetic sugarcane bagasse activated carbon	2–10*	5	120	36.14	PSO	Langmuir	[39]
Manganese ferrite/graphene oxide nanocomposites	8	–	270	89.29	PSO	Langmuir	[40]
Magnetic rice husk ash	7	10	10	150.53	PSO	Langmuir	[44]
Magnetically modified black cumin press cake	11	0.6	1,440	454.55	PSO	Langmuir	This study

*No significant effect in that pH range, PSO: pseudo-second-order kinetic model.

Table 5
Removal of methylene blue on MNYBC using real water samples (volume 25 mL, adsorbent amount 15 mg, contact time 1,440 min, pH 11, $n = 3$)

Sample	Spiked (mg/L)	Removal efficiency (%)
Distilled water	0	–
	1	91.4 ± 1.2
	10	98.2 ± 1.7
	100	97.8 ± 2.2
Tap water	0	–
	1	98.5 ± 1.5
	10	96.6 ± 2.3
	100	91.4 ± 1.4
Wastewater	0	–
	1	93.8 ± 1.7
	10	96.7 ± 3.2
	100	53.8 ± 4.3

to the bare adsorbent, only a change in the optimum pH range and a slight decrease in the maximum adsorbent capacity were observed (Figs. S2 and S3). The decrease in adsorbent capacity could be caused by magnetite particles occupying the pores on the surface of the bare adsorbent. With this modification, the separation of the MNYBC from the aqueous solution was successfully executed using a magnetic field, resulting in an increase in the removal efficiencies. Furthermore, the modification did not have a significant negative effect on the adsorbent capacity.

4. Conclusion

To eliminate MB from an aqueous medium, the surface of agricultural waste material - black cumin pressed cakes - was modified with magnetite nanoparticles. The optimum working pH was found to be 11. The optimum dosage for MNYBC computed as 0.6 g/L. It was found that adsorption was quite fast. It reached 87.78% ± 3.14% at 20 min and 99.40% ± 0.05% at 1,440 min. It is thought that higher uptake efficiency would be achieved in a shorter time when higher adsorbent dosages are used. The highest coefficient of determination seemed to fit the pseudo-second-order kinetic model. The positive enthalpy value shows that the adsorption was endothermic, the positive entropy value defines the increased randomness and the negative Gibbs free energy value highlights spontaneous and favorable adsorption. adsorption took place on a homogeneous surface with a monolayer. The highest desorption efficiency was calculated to be 49.21% ± 0.75% by ethanol. It is believed that desorption efficiency was low because chemical bonds played a role in the adsorption.

Toxic and hazardous chemicals were not used in the preparation of the adsorbent. The uptake of MB from aqueous solutions was successfully accomplished. As a result, an environmentally friendly, easily prepared, cheap adsorbent has been developed. For further research, the prepared magnetite-coated adsorbent could apply to column studies by changing the dimensions of the support material.

In addition, studies could be made to remove various contaminants (pesticides, heavy metals, drug metabolites, etc.) or their preconcentration before measurements.

Acknowledgements

This study is supported by Ege University Scientific Research Projects Coordination Unit [Project Number: 2017 FEN 074].

Declaration of competing interest

The author declares that there are no conflicts of interest regarding the publication of this article.

References

[1] V.K. Gupta, R. Kumar, A. Nayak, T.A. Saleh, M.A. Barakat, Adsorptive removal of dyes from aqueous solution onto carbon nanotubes: a review, Adv. Colloid Interface Sci., 193–194 (2013) 24–34.
[2] M.T. Yagub, T.K. Sen, S. Afroze, H.M. Ang, Dye and its removal from aqueous solution by adsorption: a review, Adv. Colloid Interface Sci., 209 (2014) 172–184.
[3] G. Crini, Non-conventional low-cost adsorbents for dye removal: a review, Bioresour. Technol., 97 (2006) 1061–1085.
[4] V.K. Gupta, S. Khamparia, I. Tyagi, D. Jaspal, A. Malviya, Decolorization of mixture of dyes: a critical review, Global J. Environ. Sci. Manage., 1 (2015) 71–94.
[5] Z. Salahshoor, A. Shahbazi, Review of the use of mesoporous silicas for removing dye from textile wastewater, Eur. J. Environ. Sci., 4 (2014) 116–130.
[6] J. Ye, S. Liu, M. Tian, W. Li, B. Hu, W. Zhou, Q. Jia, Preparation and characterization of magnetic nanoparticles for the on-line determination of gold, palladium, and platinum in mine samples based on flow injection micro-column preconcentration coupled with graphite furnace atomic absorption spectrometry, Talanta, 118 (2014) 231–237.
[7] N. Tara, M.A. Abomuti, F.M. Alshareef, O. Abdullah, E.S. Allehyani, S.A. Chaudhry, S. Oh, *Nigella sativa*-manganese ferrite-reduced graphene oxide-based nanomaterial: a novel adsorbent for water treatment, Molecules, 28 (2023) 5007, doi: 10.3390/molecules28135007.
[8] H. Singh, G. Chauhan, A.K. Jain, S.K. Sharma, Adsorptive potential of agricultural wastes for removal of dyes from aqueous solutions, J. Environ. Chem. Eng., 5 (2017) 122–135.
[9] M.A. Malik, L. AlHarbi, A. Nabi, K.A. Alzahrani, K. Narasimharao, M.R. Kamli, Facile synthesis of magnetic *Nigella sativa* seeds: advances on nano-formulation approaches for delivering antioxidants and their antifungal activity against *Candida albicans*, Pharmaceutics, 15 (2023) 642, doi: 10.3390/pharmaceutics15020642.
[10] O.I. Ali, E.R. Zaki, M.S. Abdalla, S.M. Ahmed, Mesoporous Ag-functionalized magnetic activated carbon-based agro-waste for efficient removal of Pb(II), Cd(II), and micro-organisms from wastewater, Environ. Sci. Pollut. Res., 30 (2023) 53548–53565.
[11] M. Bagherzadeh, B. Aslibeiki, N. Arsalani, Preparation of Fe_3O_4/vine shoots derived activated carbon nanocomposite for improved removal of Cr(VI) from aqueous solutions, Sci. Rep., 13 (2023) 3960, doi: 10.1038/s41598-023-31015-x.
[12] S. Sismanoglu, M.K. Akalin, G.O. Akalin, F. Topak, Effective removal of cationic dyes from aqueous solutions by using black cumin (*Nigella sativa*) seed pulp and biochar, BioResources, 18 (2023) 3414–3439.
[13] S. Rakass, A. Mohmoud, H.O. Hassani, M. Abboudi, F. Kooli, F. Al Wadaani, Modified *Nigella sativa* seeds as a novel efficient natural adsorbent for removal of methylene blue dye, Molecules, 23 (2018) 1950, doi: 10.3390/molecules23081950.
[14] S.I. Siddiqui, G. Rathi, S.A. Chaudhry, Acid washed black cumin seed powder preparation for adsorption of methylene blue dye from aqueous solution: thermodynamic, kinetic and isotherm studies, J. Mol. Liq., 264 (2018) 275–284.
[15] S.I. Siddiqui, S.A. Chaudhry, *Nigella sativa* plant-based nanocomposite-$MnFe_2O_4$/BC: an antibacterial material for water purification, J. Cleaner Prod., 200 (2018) 996–1008.
[16] S.I. Siddiqui, O. Manzoor, Mohd. Mohsin, S.A. Chaudhry, *Nigella sativa* seed-based nanocomposite-MnO_2/BC: an antibacterial material for photocatalytic degradation, and adsorptive removal of dye from water, Environ. Res., 171 (2019) 328–340.
[17] S.I. Siddiqui, F. Zohra, S.A. Chaudhry, *Nigella sativa* seed based nanohybrid composite-Fe_2O_3–SnO_2/BC: a novel material for enhanced adsorptive removal of methylene blue from water, Environ. Res., 178 (2019) 108667, doi: 10.1016/j.envres.2019.108667.
[18] N. Tara, S.I. Siddiqui, R.K. Nirala, N.K. Abdulla, S.A. Chaudhry, Synthesis of antibacterial, antioxidant and magnetic *Nigella sativa*-graphene oxide-based nanocomposite BC-GO@Fe_3O_4 for water treatment, Colloid Interface Sci. Commun., 37 (2020) 100281, doi: 10.1016/j.colcom.2020.100281.
[19] P.M. Thabede, N.D. Shooto, T. Xaba, E.B. Naidoo, Adsorption studies of toxic cadmium(II) and chromium(VI) ions from aqueous solution by activated black cumin (*Nigella sativa*) seeds, J. Environ. Chem. Eng., 8 (2020) 104045, doi: 10.1016/j.jece.2020.104045.
[20] Y. İşlek Coşkun, Biosorption of copper by a natural byproduct material: pressed black cumin cakes, Anal. Lett., 53 (2020) 1247–1265.
[21] A. Pholosi, E.B. Naidoo, A.E. Ofomaja, Enhanced arsenic(III) adsorption from aqueous solution by magnetic pine cone biomass, Mater. Chem. Phys., 222 (2019) 20–30.
[22] A. Choudhry, A. Sharma, T.A. Khan, S.A. Chaudhry, Flax seeds based magnetic hybrid nanocomposite: an advance and sustainable material for water cleansing, J. Water Process Eng., 42 (2021) 102150, doi: 10.1016/j.jwpe.2021.102150.
[23] L. Chen, B. Li, Magnetic molecularly imprinted polymer extraction of chloramphenicol from honey, Food Chem., 141 (2013) 23–28.
[24] Z. Heidarinejad, O. Rahmanian, M. Fazlzadeh, M. Heidari, Enhancement of methylene blue adsorption onto activated carbon prepared from date press cake by low frequency ultrasound, J. Mol. Liq., 264 (2018) 591–599.
[25] A.S. Franca, L.S. Oliveira, A.A. Nunes, C.C.O. Alves, Microwave assisted thermal treatment of defective coffee beans press cake for the production of adsorbents, Bioresour. Technol., 101 (2010) 1068–1074.
[26] A.A. Nunes, A.S. Franca, L.S. Oliveira, Activated carbons from waste biomass: an alternative use for biodiesel production solid residues, Bioresour. Technol., 100 (2009) 1786–1792.
[27] D.L. Nunes, A.S. Franca, L.S. Oliveira, Use of *Raphanus sativus* L press cake, a solid residue from biodiesel processing, in the production of adsorbents by microwave activation, Environ. Technol., 32 (2011) 1073–1083.
[28] B. Geng, Z. Jin, T. Li, X. Qi, Preparation of chitosan-stabilized Fe(0) nanoparticles for removal of hexavalent chromium in water, Sci. Total Environ., 407 (2009) 4994–5000.
[29] H.V. Tran, L.D. Tran, T.N. Nguyen, Preparation of chitosan/magnetite composite beads and their application for removal of Pb(II) and Ni(II) from aqueous solution, Mater. Sci. Eng. C, 30 (2010) 304–310.
[30] H.Y. Huang, Y.T. Shieh, C.M. Shih, Y.K. Twu, Magnetic chitosan/iron (II, III) oxide nanoparticles prepared by spray-drying, Carbohydr. Polym., 81 (2010) 906–910.
[31] R.A. Al-Husseiny, S.E. Ebrahim, Effective removal of methylene blue from wastewater using magnetite/geopolymer composite: synthesis, characterization and column adsorption study, Inorg. Chem. Commun., 139 (2022) 109318, doi: 10.1016/j.inoche.2022.109318.
[32] B. Stephen Inbaraj, B.H. Chen, Dye adsorption characteristics of magnetite nanoparticles coated with a biopolymer poly (γ-glutamic acid), Bioresour. Technol., 102 (2011) 8868–8876.

[33] Y.A. Teymur, F. Güzel, Ultra-efficient removal of methylene blue, oxytetracycline, and lead(II) by activated carbon derived from black cumin (*Nigella sativa*) processing solid waste, J. Water Process Eng., 54 (2023) 103940, doi: 10.1016/j.jwpe.2023.103940.
[34] K. Narasimharao, S. Al-Thabaiti, H.K. Rajor, M. Mokhtar, A. Alsheshri, S.Y. Alfaifi, S.I. Siddiqui, N.K. Abdulla, Fe_3O_4@ date seeds powder: a sustainable nanocomposite material for wastewater treatment, J. Mater. Res. Technol., 18 (2022) 3581–3597.
[35] N. Fiol, I. Villaescusa, Determination of sorbent point zero charge: usefulness in sorption studies, Environ. Chem. Lett., 7 (2009) 79–84.
[36] T.M. Petrova, L. Fachikov, J. Hristov, The magnetite as adsorbent for some hazardous species from aqueous solutions: a review, Chem. Phys., 3 (2011) 134–152.
[37] J.-M. Lee, D.-S. Lim, S.-H. Jeon, D.H. Hur, Zeta potentials of magnetite particles and alloy 690 surfaces in alkaline solutions, Materials, 13 (2020) 3999, doi: 10.3390/ma13183999.
[38] S.I. Siddiqui, S.A. Chaudhry, Nanohybrid composite Fe_2O_3-ZrO_2/BC for inhibiting the growth of bacteria and adsorptive removal of arsenic and dyes from water, J. Cleaner Prod., 223 (2019) 849–868.
[39] W. Jiang, L. Zhang, X. Guo, M. Yang, Y. Lu, Y. Wang, Y. Zheng, G. Wei, Adsorption of cationic dye from water using an iron oxide/activated carbon magnetic composites prepared from sugarcane bagasse by microwave method, Environ. Technol. U.K., 42 (2021) 337–350.
[40] L. Thi Mong Thy, N. Hoan Kiem, T. Hoang Tu, L. Minh Phu, D. Thi Yen Oanh, H. Minh Nam, M. Thanh Phong, N.H. Hieu, Fabrication of manganese ferrite/graphene oxide nanocomposites for removal of nickel ions, methylene blue from water, Chem. Phys., 533 (2020) 110700, doi: 10.1016/j.chemphys.2020.110700.
[41] Y. Kismir, A.Z. Aroguz, Adsorption characteristics of the hazardous dye Brilliant Green on Saklıkent mud, Chem. Eng. J., 172 (2011) 199–206.
[42] T.D. Çiftçi, Adsorptive properties of Fe_3O_4/Ni/Ni_xB nanocomposite coated nutshell for the removal of arsenic(III) and arsenic(V) from waters, Cogent Chem., 3 (2017) 1–15.
[43] M. Ghaedi, H. Hossainian, M. Montazerozohori, A. Shokrollahi, F. Shojaipour, M. Soylak, M.K. Purkait, A novel acorn-based adsorbent for the removal of brilliant green, Desalination, 281 (2011) 226–233.
[44] V.S. Mane, I.D. Mall, V.C. Srivastava, Kinetic and equilibrium isotherm studies for the adsorptive removal of Brilliant Green dye from aqueous solution by rice husk ash, J. Environ. Manage., 84 (2007) 390–400.
[45] I. Langmuir, The adsorption of gases on plane surfaces of glass, mica and platinum, J. Am. Chem. Soc., 40 (1918) 1361–1403.
[46] N.D. Hutson, R.T. Yang, Theoretical basis for the Dubinin–Radushkevich (D-R) adsorption isotherm equation, Adsorption, 3 (1997) 189–195.

Supporting information

S1. Thermodynamic equations

$$\ln K_L = -\frac{\Delta H^\circ}{RT} + \frac{\Delta S^\circ}{R} \quad \text{(S1)}$$

$$\Delta G^\circ = -RT \ln K_L \quad \text{(S2)}$$

$$\Delta G^\circ = \Delta H^\circ - T\Delta S^\circ \quad \text{(S3)}$$

where ΔG is the free energy change (kJ/mol), R is the gas constant (8.314 J/mol·K), K_L (L/mol) is the thermodynamic equilibrium constant, and T is the temperature (K), and ΔH (kJ/mol) and ΔS (J/mol·K) are the enthalpy and entropy changes of the system, respectively.

The K_L values were found from the ratio of the methylene blue dye mass (mg) and equilibrium methylene blue dye concentration in the solution (mg/L). The parameters of ΔH and ΔS were obtained from the slope and the intercept of the van't Hoff graph between $\ln K_L$ and $1/T$, respectively [S1–S3].

S2. Isotherm models and equations

The Langmuir isotherm is based on the recognition that adsorption occurred at specific homogenous sites within the adsorbent, while the Freundlich isotherm notes the acceptance of a heterogeneous surface with a non-uniform distribution of heat of adsorption over the surface. The Dubinin–Radushkevich isotherm expresses the mechanism of adsorption onto a heterogeneous surface [S4–S7]. The linearized equations:

S2.1. Langmuir equation

$$\frac{C_2}{q} = \left(\frac{1}{Q_{max}}\right) C_2 + \frac{1}{bQ_{max}} \quad \text{(S4)}$$

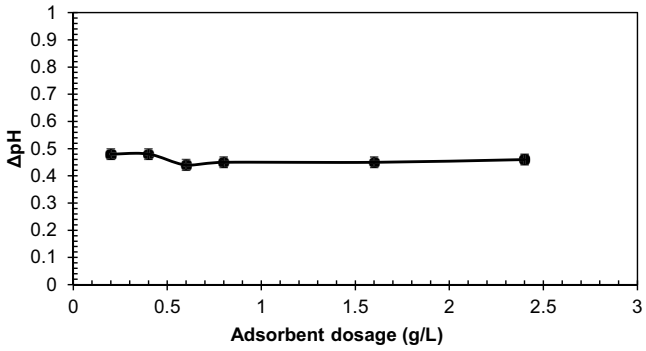

Fig. S1. Correlation of adsorbent dosage and pH change before and after adsorption.

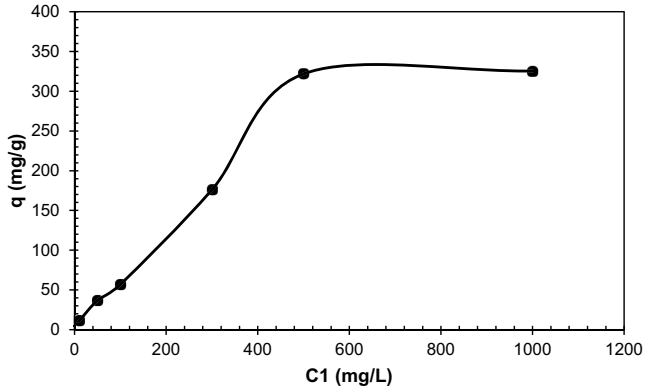

Fig. S3. Graph of adsorbent capacity for MNYBC.

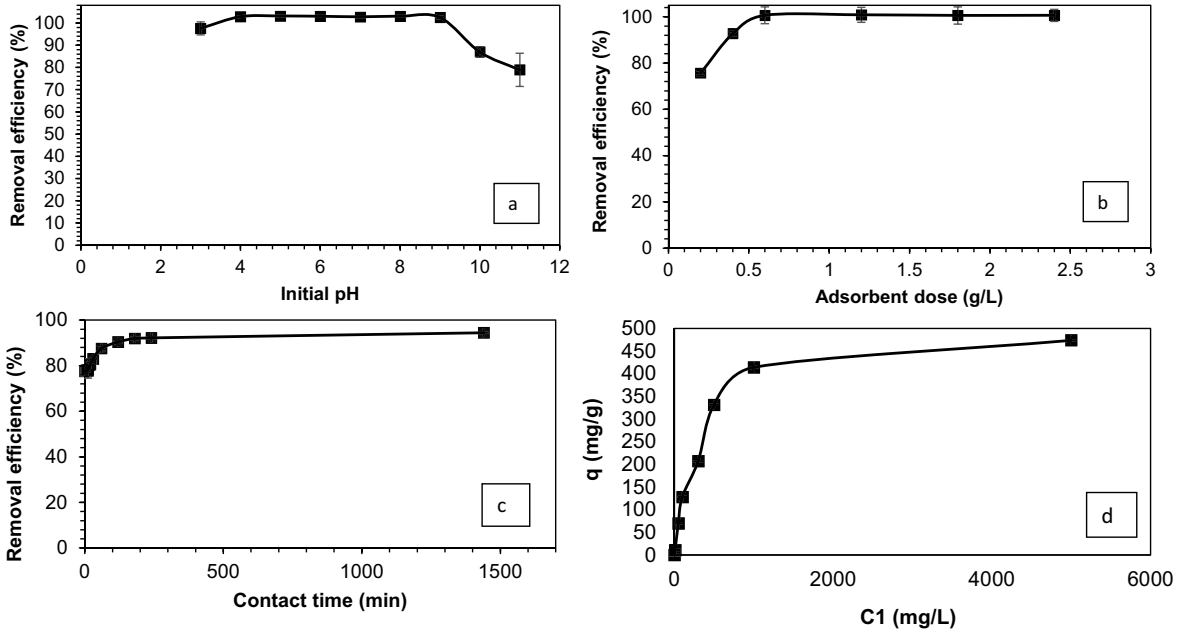

Fig. S2. Graphs of bare adsorbent (a) pH, (b) adsorbent dose, (c) contact time, and (d) adsorbent capacity

Table S1
Parameters determined for the Langmuir, Freundlich, and Dubinin–Radushkevich isotherms for bare adsorbent

Isotherm models		
Langmuir isotherm	Q_{max} (mg/g)	476.19
	b (L/mg)	0.007952
	R^2	0.9987
	Separation factor (R_L)	0.988–0.032
Freundlich isotherm	$1/n$	0.4607
	K (mg/g)	17.0686
	R^2	0.8045
Dubinin–Radushkevich isotherm	E (kJ/mol)	3.74
	Q_m (mol/g)	0.0036
	K (mol²/kJ)	0.0357
	R^2	0.7268

Table S2
Thermodynamic constants for the adsorption of methylene blue by bare adsorbent

Temperature (K)	Standard enthalpy changes (kJ/mol)	Standard entropy changes (J/mol·K)	Gibbs free energy changes (kJ/mol)
298	102.20	23.43	–7.031
303			–7.542
323			–9.586
343			–11.63

$$R_L = \left(\frac{1}{1+bC_1}\right) \quad \text{(S5)}$$

S2.2. Freundlich equation

$$\log q = \log K + \frac{1}{n}\log C_2 \quad \text{(S6)}$$

S2.3. Dubinin–Radushkevich equation

$$\ln Q = \ln Q_m - k\varepsilon^2 \quad \text{(S7)}$$

$$E = \left(2k\right)^{-0.5} \quad \text{(S8)}$$

where C_1 is the initial concentration of the solution (mg/L), C_2 is the equilibrium concentration of the methylene blue (MB) solution (mg/L), q is the mass of adsorbed MB dye/mass of adsorbent (mg/g), b is the Langmuir constant (L/mg), R_L is the separation factor, Q_{max} is the monolayer adsorption capacity (mg/g), K is the Freundlich constant ((mg/g)(L/mg)^n), and $1/n$ is a dimensionless Freundlich constant for the adsorption intensity of the process. The linear graph of the Langmuir and Freundlich isotherm models was drawn by plotting C_2/q against C_2 and between log$q$ and logC_2, respectively. ε is the Polanyi potential ($RT\ln(1 + 1/C_2)$), Q is the moles of MB adsorbed per unit weight of adsorbent (mol/g), Q_m is the adsorption capacity (mol/g), k is a constant related to adsorption energy (mol²/kJ²), R is the gas constant (kJ/mol·K), T is the absolute temperature (K), and E is the mean free energy of adsorption (kJ/mol²).

S2.4. Debye–Scherrer equation

$$D = \frac{K\lambda}{\beta\cos\theta} \quad \text{(S9)}$$

where K is Scherrer constant (K = 0.9), λ is wavelength of X-ray radiation (λ = 0.15406 nm), β is full width at half maxima (FWHM) (radians), θ is Bragg's angle (radians).

References

[S1] Y. Bulut, H. Aydin, A kinetics and thermodynamics study of methylene blue adsorption on wheat shells, Desalination, 194 (2006) 259–267.

[S2] V.S. Mane, I.D. Mall, V.C. Srivastava, Kinetic and equilibrium isotherm studies for the adsorptive removal of Brilliant Green Dye from aqueous solution by rice husk ash, J. Environ. Manage., 84 (2007) 390–400.

[S3] V.S. Mane, P.V.V. Babu, Studies on the adsorption of Brilliant Green dye from aqueous solution onto low-cost NaOH treated saw dust, Desalination, 273 (2011) 321–329.

[S4] Y. Kismir, A.Z. Aroguz, Adsorption characteristics of the hazardous dye Brilliant Green on Saklıkent mud, Chem. Eng. J., 172 (2011) 199–206.

[S5] T.D. Çiftçi, Adsorptive properties of Fe_3O_4/Ni/Ni_xB nanocomposite coated nutshell for the removal of arsenic(III) and arsenic(V) from waters, Cogent Chem., 3 (2017) 1–15.

[S6] I. Langmuir, The adsorption of gases on plane surfaces of glass, mica and platinum, J. Am. Chem. Soc., 40 (1918) 1361–1403.

[S7] N.D. Hutson, R.T. Yang, Theoretical basis for the Dubinin–Radushkevich (D-R) adsorption isotherm equation, Adsorption, 3 (1997) 189–195.